Small-scale Finite Element Modelling of the Plastic Deformation Zone in the Incremental Forming Process

P. Eyckens[1], A. Van Bael[1,2], R. Aerens[3], J. Duflou[3], P. Van Houtte[1]

[1]*MTM, Katholieke Universiteit Leuven – Kasteelpark Arenberg 44, B-3001 Heverlee, Belgium. e-mails: Philip.Eyckens@mtm.kuleuven.be; Albert.VanBael@mtm.kuleuven.be; Paul.VanHoutte@mtm.kuleuven.be.*

[2]*IWT, KHLim (Limburg Catholic University College), Campus Diepenbeek, Agoralaan gebouw B, bus 3, B-3590 Diepenbeek, Belgium.*

[3]*PMA, Katholieke Universiteit Leuven – Celestijnenlaan 300 B, B-3001 Heverlee, Belgium. e-mails: Richard.Aerens@sirris.be; Joost.Duflou@mech.kuleuven.be.*

ABSTRACT: In this paper, the Finite Element submodelling technique is applied to model the small plastic zone in the Incremental Forming process with an adequately fine (sub-millimetre) mesh at a computationally acceptable cost. The focus lies on the distribution of the contact pressure between sheet and forming tool. Different forming conditions of truncated cones are considered. Results show that the contact consists of two distinguishable parts. The obtained insights can be applied in the physical modelling of forming forces, which allows improving part accuracy through compensation for the mechanical stiffness of the forming machine.

Key words: Incremental forming, Contact pressure distribution, Finite Elements, Submodelling technique.

1 INTRODUCTION

The Implicit Finite Element (FE) simulations of the Single Point Incremental Forming (SPIF) process have been shown to be very computationally intensive. This is, amongst other reasons, due to the constantly changing contact between the tool and the metal sheet. In the past, partial FE models with non-physical boundary conditions (BC's), such as symmetry BC's, and relatively coarse meshes have been used to model the process within reasonable calculation times [1].

In this paper, a new strategy is presented to model the small plastic zone under the SPIF forming tool in a more accurate manner. Only a small piece of the unclamped sheet is considered in the FE model, which allows for a much finer mesh with respect to the forming tool radius, while retaining reasonable calculation times. The FE submodelling technique [2] allows the BC's on the edges of this model to be physically meaningful. The same approach has been used to study out-of-plane shear in SPIF [3].

This paper describes FE models on different scales for the SPIF fabrication of truncated cones of AA3003-O aluminium alloy sheet under different process conditions. The forming force components are compared to experimental measurements, and the distribution of the contact pressure under the forming tool is investigated for different process conditions. The resulting insights are useful for the physical modelling of the forming force, which can be used to compensate for the machine stiffness and consequently to increase the accuracy of SPIF parts.

2 FINITE ELEMENT MODEL DESCRIPTION

2.1 The SPIF case studies

In the present study, four different Incremental Forming processes of truncated cones are modelled with FE simulations. An overview of the main experimental parameters is given in table 1.

Table1. Parameters of the SPIF processes

Name:	*c20d10*	*c20d25*	*c60d10*	*c60d25*
Wall angle	20°	20°	60°	60°
Tool diameter (mm)	10.0	25.0	10.0	25.0
Scallop height (μm)	15.0	15.0	18.5	18.5
Step size (mm)	0.2647	0.4188	0.7440	1.1769
Number of contours	45	30	50	45

In all cases, a succession of circular tool contours (with diminishing radius) was used to form the cones. The main differences lie in the wall angle

(20° or 60°) and the diameter of the forming tool (10 or 25mm). The scallop height, i.e. the resulting roughness height on the cone inner wall due to the tool contact, is 15µm and 18.5µm for the cones with a 20° and 60° wall angle, respectively. The (vertical) step size of the tool in-between contours is deduced from the previous parameters. For all cones, the radius of the first tool path contour was 75mm, and a backing plate with circumferential orifice with a radius of 91mm was used. The material is the aluminium alloy AA3003-O (annealed state) with a sheet thickness of 1.2mm.

2.2 The FE global model and submodels

Each of the 4 SPIF processes is simulated with 3 implicit FE models at different scales. In all cases the sheet is modelled as several layers of linear brick elements, while the forming tool is modelled as an analytical rigid sphere. Isotropic hardening (Swift-type) of the sheet is assumed, in combination with the isotropic Von Mises yield criterion. Coulomb friction with a friction coefficient of 0.05 is used. First, a 40° pie model (global model: '*G*') with a relative coarse mesh, containing 3 layers of elements and (non-physical) symmetry boundary conditions was used, as shown in figure 1.

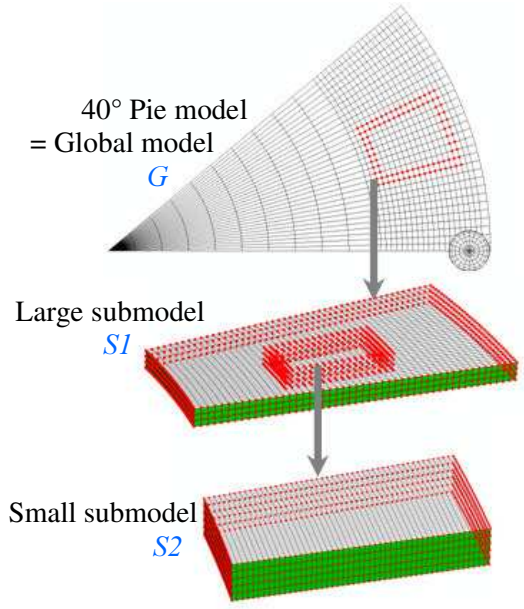

Fig. 1. The mesh of the FE models.

Next, a small piece of the sheet was modelled, i.e. the large submodel *S1*. The BC's on the edges of this model were obtained as a linear interpolation of the nodal solution of the global model, shown schematically in figure 1 with an arrow. The imposed tool path remains unchanged. This procedure is repeated to model the process at an even smaller scale, resulting in the small submodel *S2*, in which 5 layers of elements are used.

Table 2 shows the model and element dimensions at the 3 different scales. The centre of both submodels *S1* and *S2* was chosen depending on the cone wall angle, as to obtain a steady state in forming forces. The calculation times for any of these models was about 1 to 2 days on a 16GB-RAM 2.4GHz CPU.

Table2. FE model parameters of the SPIF processes

Model dimensions	*G*	91.0mm * 40.0° * 1.2mm
	S1	21.0mm * 10.5° * 1.2mm
	S2	7.0mm * 3.3° * 1.2mm
Approx. element dimensions (mm)	*G*	1.2 * 1.4 * 0.4
	S1	0.3 * 0.4 * 0.4
	S2	0.10 * 0.14 * 0.24
Approx. number of elements	*G*	4300
	S1	5100
	S2	8600
Distance from cone centre to submodel centre (*S1* & *S2*)	*c20dxx*	55.0mm
	c60dxx	65.0mm

3 RESULTS

3.1 Forming force components

Experimental and modelled forming force components are shown in table 3 for the contour during which the tool path moves closest to the centre of both submodels *S1* and *S2*.

Table3. Average force components (unit: N)

		Fz	*Fr*	*Ft*
c20d10 cont. 29	*exp*	283,9	-37,3	58,2
	G	303,1	-16,7	37,9
	S1	290,2	-18,8	46,1
	S2	307,3	-16,9	52,2
c20d25 cont. 18	*exp*	329,6	6,6	54,6
	G	380,5	8,6	37,9
	S1	328,7	2,2	39,7
	S2	298,1	-0,6	37,9
c60d10 cont. 24	*exp*	509,4	176,5	106,3
	G	691,1	248,0	141,0
	S1	620,5	209,5	158,9
	S2	606,2	180,4	164,6
c60d25 cont. 16	*exp*	754,1	339,0	119,2
	G	979,5	422,0	212,9
	S1	875,0	377,3	207,2
	S2	*446,1*	*39,9*	*89,4*

The component *Fz* lies along the direction perpendicular to the initial sheet surface, while *Fr* and *Ft* are the components along the local radial and

tool movement direction, respectively. During a contour, the predicted force components oscillate due to the meshing of the sheet. The amplitude of these oscillations is in general smaller in the centre of the submodels compared to the global model, thanks to the finer mesh [3]. The averages in table 3 are calculated in the central part (1/3rd) of each model, to exclude spurious force oscillations at the model edges. Results of the *S2*-model of *c20d25* are shown in italic in table 3, since the contact zone appeared to be too large to be fully covered by this model.

The components *Fz* and *Fr* are usually overpredicted by the FE models. However, there is a trend of better predictions when a smaller submodel (with finer mesh) is used. This is most evident in the *Fz*-component of the cones with the higher wall angle of 60°, e.g. the relative overprediction for the cone *c60d10* drops from 135% for the *G*-model to 119% for the *S2*-model. Also, the experimental and simulated *Fr*-components of *c20d10* are found to be negative. It means that the tool is pushed outwards rather than in the direction of the cone centre.

The relative error of the *Ft*-component prediction is generally the largest, and in all cases except *c20d10*, there is no significant improvement when a smaller FE model is used. This can be attributed to the simple contact model used, as this component is mainly due to frictional contact shear forces.

3.2 The distribution of tool contact pressure

The simulated contact area between the tool and the sheet oscillates for the same reason as the force components. Table 4 gives the averaged contact area *A* obtained by the same averaging procedure as used for the forces. It also gives the variation in contact area *ΔA*, i.e. the maximal minus minimal value of contact area for the given contour.

Table4. Average contact area and variation (unit: mm²)

		A	*ΔA*
c20d10 cont 29	*G*	2,4	1,7
	S1	0,7	0,3
	S2	1,1	0,3
c20d25 cont 18	*G*	6,2	3,5
	S1	1,4	0,3
	S2	1,4	0,3
c60d10 cont 24	*G*	15,3	8,2
	S1	2,1	0,8
	S2	2,1	0,6
c60d25 cont 16	*G*	36,6	17,8
	S1	7,9	1,2
	S2	*2,5*	*2,1*

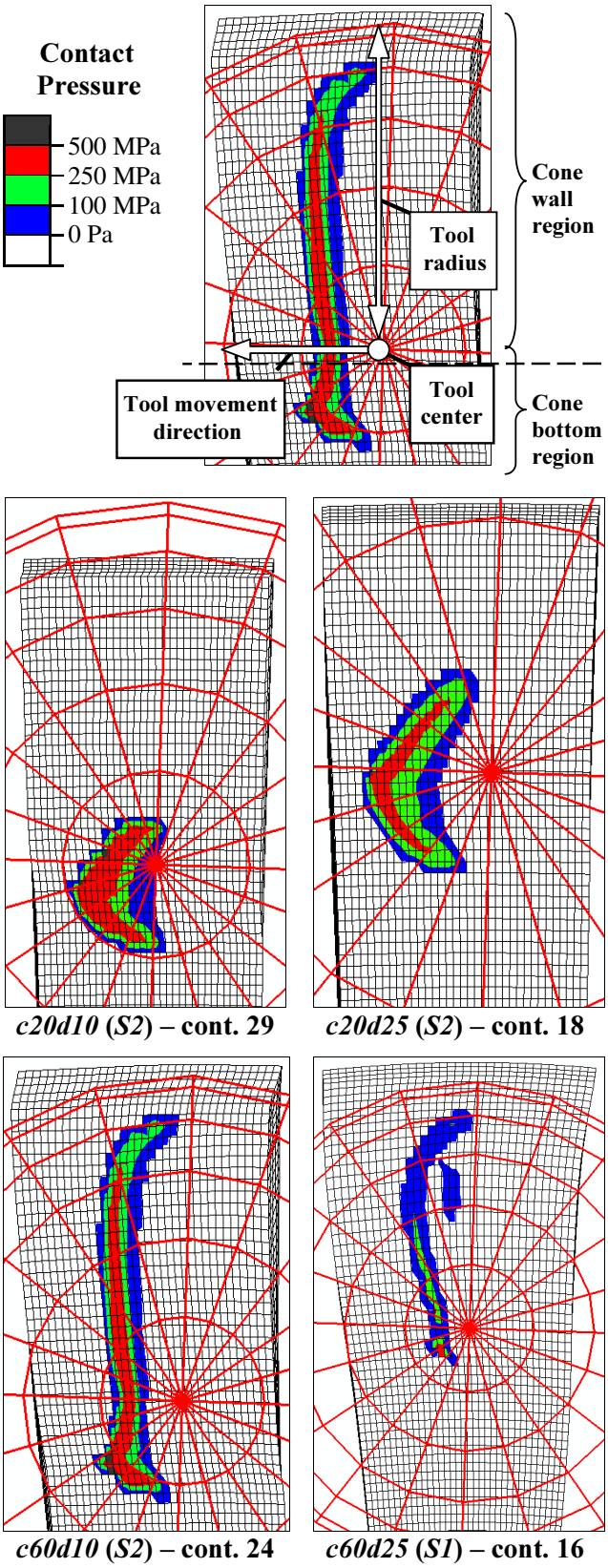

Fig. 2. The distribution of contact pressure under the tool. The view is perpendicular to the initial sheet surface.

It can be seen that for both submodels practically identical results are found, while the *G*-model yields much higher values of A and ΔA. It can thus be argued that the coarse mesh of this model results in an overprediction of the contact area. Figure 2 shows the distribution of the contact pressure for all four cases. The position, size and movement direction of the tool with respect to the cone wall and bottom region are clarified in the upper part of figure 2.
The contact in the cone wall region appears approximately to be a line contact for the cones with a wall angle of 60°. There is also a non-negligible sickle-shaped contact in the cone bottom region. For the cones with the low wall angle of 20°, the contact in the cone bottom region is the dominant feature, while the contact in the cone wall region is much less pronounced.
Note that the point on the tool surface directly below the tool centre is not or barely in contact with the sheet.

3.3 Cone inner surface geometry

Figure 3 illustrates the geometry of the inner surface of the cone *c20d10* in the tool contact zone and compares it to the distribution of contact pressure.

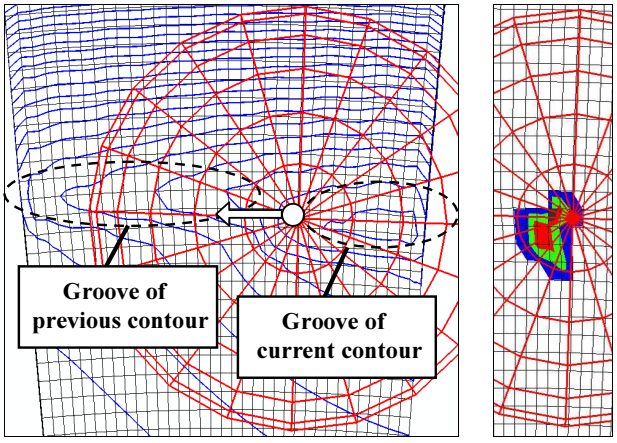

Fig. 3. (left) Contours of equal height (i.e. along the z-direction) of the inner cone surface, with intervals of 0.05mm, and (right) the contact pressure. The view and the colour code for the contact pressure are the same as in figure 2.

It can be seen that a groove in the inner sheet surface is formed as the tool moves. The groove that was formed by the tool during its previous contour can also be seen. This groove is situated more near the cone wall, since the radius of the previous circular contour was larger. During the tool movement, the groove of the previous contour is displaced in the direction of the cone centre, resulting in contact in the cone bottom region.

CONCLUSIONS

The FE submodelling technique has been used to improve the modelling of the plastic deformation zone in the SPIF process. Although the constitutive model of the sheet was too simple to accurately predict the forming force components, the quality of the forming force predictions was improved through the use of finer, sub-millimetre meshes.
The comparison of the distribution of the contact pressure under different working conditions reveals that the contact can generally be split up into two parts. Firstly, the contact with the cone wall or *wall contact*, is well approximated as a line contact at larger wall angles, while it diminishes at small wall angles. Secondly, the contact on the cone bottom or *groove contact*, appears to be sickle-shaped. It can be attributed to the presence of a contact groove in the sheet material, formed during the previous contour of the tool. It makes an important contribution to the overall contact, even when the wall angle is as large as 60°. At very low wall angles, like 20° in the present study, it is responsible for the radial component of the forming force to become nearly zero or even negative, which means that the tool is pushed outwards instead of in the direction of the cone centre.

ACKNOWLEDGEMENTS

The authors gratefully acknowledge the financial support from the Institute for the Promotion of Innovation by Science and Technology in Flanders (IWT) and from the Interuniversity Attraction Poles Program from the Belgian State through the Belgian Science Policy agency, contract IAP6/24.

REFERENCES

1. S. He, A. Van Bael, P. Van Houtte, A. Szekerez, J. Duflou, C. Henrard, A.M. Habraken, Finite Element Modeling of Incremental Forming of Aluminum Sheets, *Advanced Materials Research* 6-8 (2005), 525-532.
2. ABAQUS User's manual, version 6.6, 2006.
3. P. Eyckens, S. He, A. Van Bael, J. Duflou and P. Van Houtte, Finite Element Based Formability Prediction of Sheets Subjected to the Incremental Forming Process, In: *Computational Plasticity IX - Fundamentals and Applications*, eds, E. Oñate, R. Owen, B. Suárez, Barcelona (2007) 529-532.